RESEARCH ARTICLE

CrossMark

Interaction between central volcanoes and regional tectonics along divergent plate boundaries: Askja, Iceland

Daniele Trippanera[1] · Joël Ruch[2] · Valerio Acocella[1] · Thor Thordarson[3] · Stefano Urbani[1]

Abstract

Activity within magmatic divergent plate boundaries (MDPB) focuses along both regional fissure swarms and central volcanoes. An ideal place to investigate their mutual relationship is the Askja central volcano in Iceland. Askja consists of three nested calderas (namely Kollur, Askja and Öskjuvatn) located within a hyaloclastite massif along the NNE-SSW trending Icelandic MDPB. We performed an extensive field-based structural analysis supported by a remote sensing study of tectonic and volcanic features of Askja's calderas and of the eastern flank of the hyaloclastite massif. In the massif, volcano-tectonic structures trend N 10° E to N 40° E, but they vary around the Askja caldera being both parallel to the caldera rim and cross-cutting on the Western side. Structural trends around the Öskjuvatn caldera are typically rim parallel. Volcanic vents and dikes are preferentially distributed along the caldera ring faults; however, they follow the NNE-SSW regional structures when located outside the calderas. Our results highlight that the Askja volcano displays a balanced amount of regional (fissure-swarm related) and local (shallow-magma-chamber related) tectonic structures along with a mutual interaction among these. This is different from Krafla volcano (to the north of Askja) dominated by regional structures and Grímsvötn (to the South) dominated by local structures. Therefore, Askja represents an intermediate tectono-magmatic setting for volcanoes located in a slow divergent plate boundary. This is also likely in accordance with a northward increase in the spreading rate along the Icelandic MDPB.

Introduction

Divergent plate boundaries are influenced by long-term tectonic activity and characterised by fissure swarms where most of the tectonic and magmatic activity occurs (e.g. Ebinger et al. 2010; Wright et al. 2012; Acocella 2014; Acocella and Trippanera 2016). The continuity of these swarms is usually interrupted by central volcanoes or volcanic complexes, with a prominent topography, more differentiated magmatic products and commonly featuring a summit caldera (e.g. Gudmundsson 1995; Sigmundsson 2006); all these features are the expression of overlapping local and regional stress fields, both magmatically induced and associated with the regional plate spreading (Gudmundsson 2006, 2011; Acocella 2014). Several authors have investigated and defined the relationships between regional rift structures, these being faults and eruptive fissures related to the fissure swarm, and the local volcanic structures, i.e. caldera ring faults and circumferential or radial volcanic fissures (Gudmundsson 1995, 1998; Acocella et al. 2002; Bosworth et al. 2003). Several studies have also investigated the geometric and structural connections (Acocella et al. 2003; Acocella 2006; Hjartardóttir et al. 2009). However, the understanding of both their temporal and spatial evolution still needs to be further developed and outstanding questions remain. For example, these regional and local domains may be interpreted as an integral part of an entire system which enhances lateral flow propagation within the volcanic system or they may be considered as overlapping trends generated by different features

✉ Daniele Trippanera
daniele.trippanera@uniroma3.it

[1] Dipartimento di Scienze, Roma Tre, Rome, Italy

[2] KAUST University, Thuwal, Saudi Arabia

[3] Faculty of Earth Sciences, University of Iceland, Reykjavik, Iceland

🙋 Springer

independently responding to the magma supply (e.g. Hartley and Thordarson 2013).

Many tectono-magmatic studies on divergent plate boundaries focus on the East African Rift System, including the Western Branch (Wadge and Burt 2011; Wauthier et al. 2015), the Main Ethiopian Rift (Acocella et al. 2003; Hutchison et al. 2015, 2016) and the Erta Ale Range (Acocella 2006; Pagli et al. 2012; Nobile et al. 2012). Instead, in Iceland, many studies have focused on observable modern day surface activity along the axial rift, such as those produced by rifting episodes within individual volcanic systems or segments of the axial rift (e.g. Björnsson et al. 1977; Tryggvason 1984; Saemundsson 1991; Rubin 1992; Buck et al. 2006; Hollingsworth et al. 2012, 2013; Sigmundsson et al. 2014; Gudmundsson et al. 2014, 2016; Ruch et al. 2016; Hjartardóttir et al. 2016a) or unrest at central volcanoes (e.g. Pagli et al. 2006; Sigmundsson et al. 2010; Hreinsdottir et al. 2014). Other studies have analysed the relationships between older, but well-exposed, regional and local volcano-tectonic structures (e.g. Walker 1958, 1963, 1974; Gautneb and Gudmundsson 1992; Forslund and Gudmundsson 1992; Gudmundsson 1995, 2006; Gudmundsson and Andrew 2007; Andrew and Gudmundsson 2008; Gudmundsson et al. 2009; Hjartardóttir et al. 2009, 2016b; Hjartardóttir and Einarsson 2015). However, despite these studies, the understanding of the structure within a central volcano, and the role of both regional and local stress components in shaping the system, is still limited. Further research in this respect will undoubtedly advance our knowledge as to how volcanic edifices grow, develop and interact with the surrounding rift structures, and how magma propagates within the complex structural framework in Iceland. Our study aims at defining the structural framework of the Askja volcano, with the objective of better understanding the interplay between central volcanoes, their magmatic systems and the regional tectonics.

Remote sensing-based studies show that the Askja volcano features ample evidence of both regional and local volcano-tectonic structures (e.g. Hjartardóttir et al. 2009; Hartley and Thordarson 2012). Furthermore, a comprehensive structural model for Askja has not yet been presented. We, thus, here provide new structural field data from the Askja volcano and merge these with new and already published remote sensing data. The combined datasets provide the basis for a better understanding of the volcano-tectonic processes from the local to regional scales.

Geologic setting

The Askja central volcano belongs to the Askja volcanic system (Thordarson and Larsen 2007) and is located in the North Volcanic Zone of Iceland, a zone which is extending at ~2 cm/year in a ~N 105° direction (Fig. 1a; DeMets et al. 2010; Sella et al. 2002; Perlt et al. 2008). The fissure swarm related to the Askja volcanic system has a nearly N-S trend (i.e. N 0°–20° E) about 40 km north of Askja, and a NNE-SSW trend immediately north of Askja. The swarm turns back to a more N-S trend south of the volcanic system (Fig. 1a). Therefore, most of the swarm is oblique to the spreading direction and only the segment immediately north of Askja is roughly perpendicular to it. Moreover, the swarm widens close to the central edifice, where the density of fractures also increases (Fig. 1b; Hjartardóttir et al. 2009). Close to Askja, the fissure-swarm margins are not well defined, being probably located west of Vesturfjöll and east of Austurfjöll, where several normal faults and volcanic fissures have been recognised (Fig. 1b; Hjartardóttir et al. 2009; Hartley and Thordarson 2012).

The Askja central volcano is thought to have been active for 200–300 ka (Brown et al. 1991; Sigvaldason 2002) and hosts at least three nested calderas located within the predominantly pre-Holocene basaltic Dyngjufjöll massif. The massif can be divided into the Vesturfjöll and Norðurfjöll sectors in the west and north, and Austurfjöll in the east (Fig. 1b; e.g. Brown et al. 1991; Hartley et al. 2016). The massif is the product of several inter-glacial, ice-confined sub-aqueous, sub-glacial and emergent basaltic eruptions that produced an 800-m thick sequence of tuffs, lapilli tuffs, hyaloclastite, pillow lava breccia and pillow lava from 300 to 7 ka (Fig. 1b; Graettinger et al. 2013; Hartley et al. 2016).

Among the three calderas, Kollur is the oldest having formed in the Pleistocene (Sigvaldason 1979), and occupies the innermost part of Norðurfjöll (Fig. 1b). Its rim is not entirely exposed and is partly obscured by the younger Holocene Askja caldera (Sigvaldason 2002). The 8-km wide Askja caldera is the largest among the three and is located in the centre of the Dyngjufjöll massif (Sigvaldason 1979; Brown et al. 1991). The caldera faults dissect mid-Holocene lava flows along the rim in Norðurfjöll, and the caldera floor is mainly covered by lavas erupted between 1362 and 1477 AD (Fig. 1b, Annertz et al. 1985; Hartley et al. 2016).

Öskjuvatn is the inner and youngest caldera. It is ~5 km wide and 150–200 m deep (Hartley and Thordarson 2012; Fridriksson 2014) and hosts the Lake Öskjuvatn (Fig. 1). The formation of this caldera was initiated by the 29–30 March 1875 rhyolitic Plinian eruption and grew over 40 years to reach its current form (Hartley and Thordarson 2012). The 1875 eruption was part of a rifting episode that took place on the Askja system between 1874 and 1876. The episode featured six basaltic fissure eruptions along the Sveinagjá graben, ~60 km north of Askja, and a possible eruption within the Norðurfjöll massif (e.g. Gudmundsson and Backstrom 1991; Hartley and Thordarson 2013).

The Askja volcano has produced more than 175 eruptions (both effusive and explosive) during the last 7 ka, more than 50 of which occurred in historical times (Hartley et al. 2016). About half (24) occurred within the
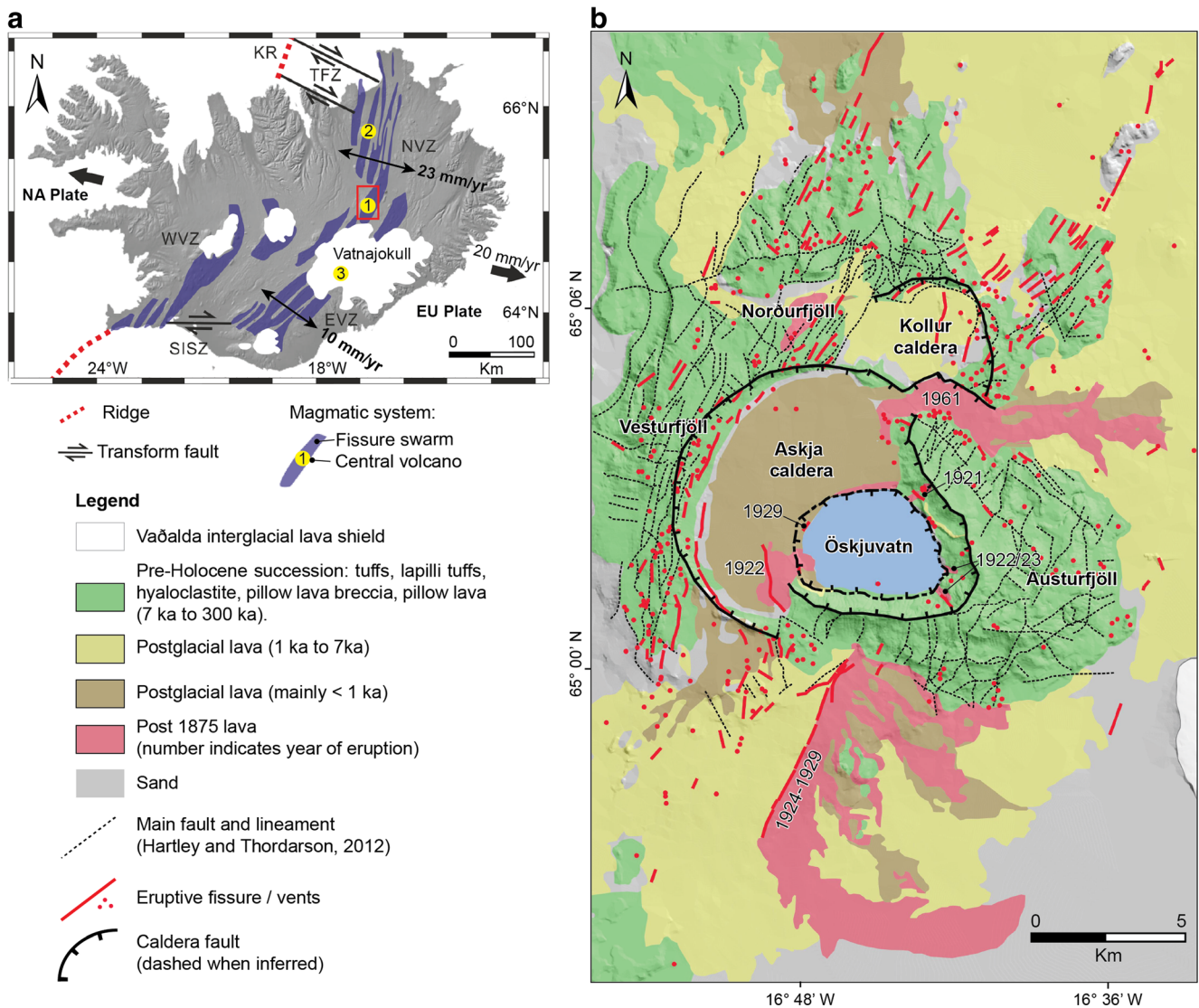
Fig. 1 **a** Map of Iceland and its volcanic zones with the locations of (1) Askja, (2) Krafla and (3) Grímsvötn central volcanoes; abbreviations are as follows: NVZ North Volcanic Zone, EVZ East Volcanic Zone, WVZ West Volcanic Zone, SISZ South Iceland Seismic Zone, TFZ Tjörnes Fracture Zone, KR Kolbeinsey Ridge. **b** Simplified geological map of the Askja volcanic complex (after Hartley and Thordarson 2012 and Hartley et al. 2016)

Askja caldera, with most of the remainder located on the flanks of the central volcano or on the fissure swarm at the foot of the massif. Small basaltic eruptions, associated with formation of scoria cones and emplacement of lava flows took place between 1921 and 1929 along the rim of the Öskjuvatn caldera. Two moderate-sized basaltic eruptions (<<1 km^3) then took place in 1922 and 1961 within the Askja caldera (Fig. 1b). A third moderate-sized eruption occurred in 1924–1929 from a 3-km long NNE-SSW-oriented fissure south of the caldera, along a regional fault belonging to the Askja fissure swarm (Fig. 1b). The historical mafic lavas and tephra range from olivine tholeiites to basaltic andesites that exhibit variability in trace element concentrations and ratios along the strike of the Askja volcanic system (Hartley and Thordarson 2013).

Askja underwent inflation until 1972 but was experiencing deflation by the time that measurements resumed in 1983 (Sturkell et al. 2006; De Zeeuw-van Dalfsen et al. 2012, 2013). Between 1983 and 1998, the subsidence rate was 7 mm/year, decreasing to 2.5–3 mm/year between 2000 and 2009. The total subsidence since 1983 is more than 75 cm (Sturkell et al. 2006). A combination of magma drainage and contraction due to cooling of a magma storage zone below the northeast rim of the Öskjuvatn caldera possibly explains both the geodetic and gravity data (De Zeeuw-van Dalfsen et al. 2005). An additional cause of deflation may be ascribed to the 6 mm/year of spreading of the fissure swarm (Sturkell and Sigmundsson 2000; Pagli et al. 2006; Sturkell et al. 2006), accommodating magma drainage from the magma storage zone (Lupi et al. 2011; De Zeeuw-van Dalfsen et al. 2012).
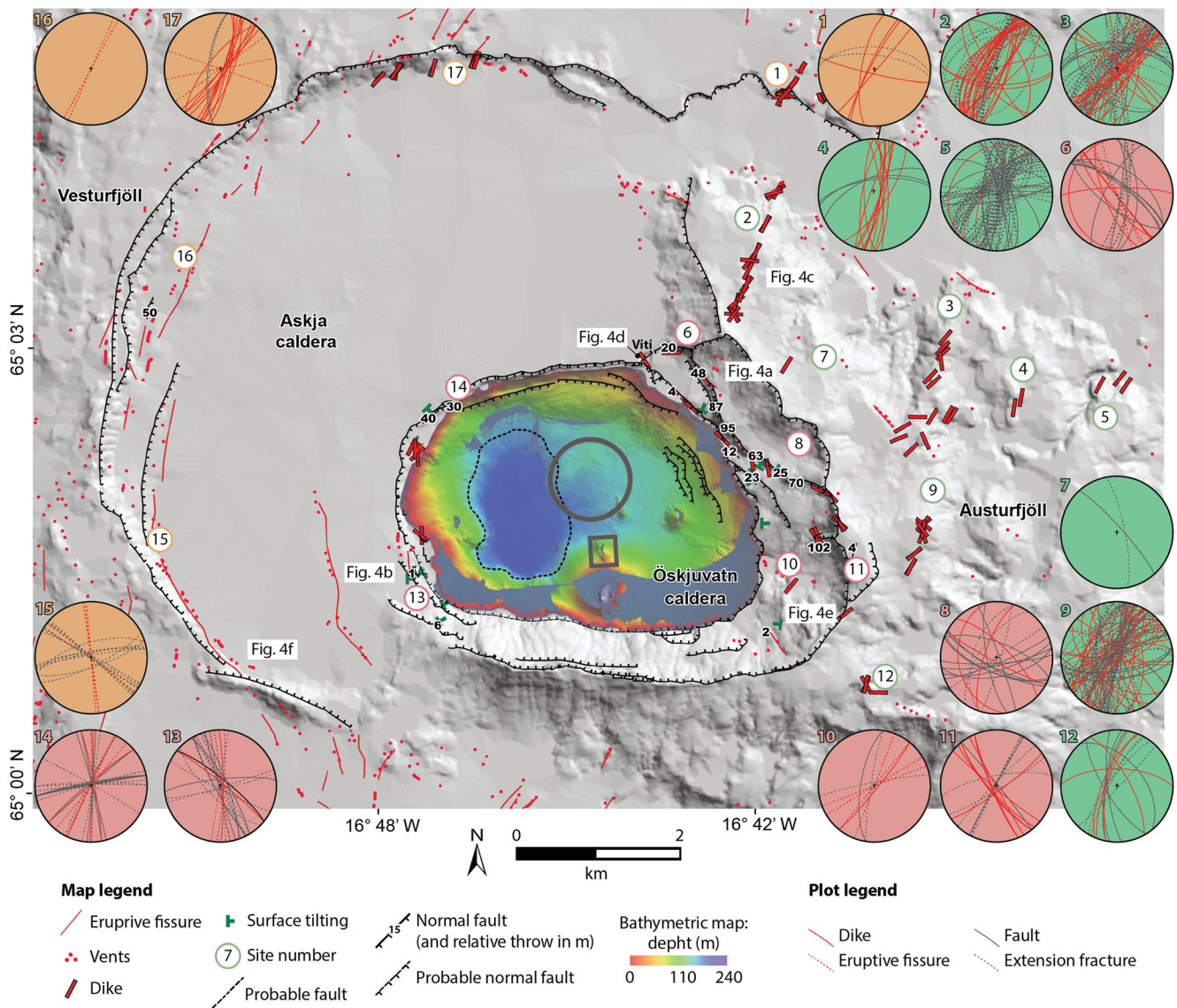
Fig. 2 Map of Askja central volcano showing the location of field measurements. Dikes are plotted according to their orientation. Bathymetric map for the Öskjuvatn caldera is from Fridriksson (2014): the grey box highlights a crater associated with a current fumarole activity, and the grey circle indicates the location of the Sò lake which formed before Öskjuvatn's lake. Viti, Viti crater. Field data are plotted on lower-hemisphere equal-area projections. Plot colours indicate that sector of the volcano: Austurfjöl (green), Askja caldera (orange) and Öskjuvatn caldera (red); location of each plot is indicated by numbers within circles

Seismic tomography reveals a main magma body with a ~ 10% of melt fraction at 5 km below sea level (b.s.l.) under Askja. Additional, but smaller, magma bodies lie between 9 and 2 km b.s.l., for a total estimated magma volume of ~ 100 km^3 (Greenfield et al. 2016).

Between 2007 and 2009, a gravity increase was detected at the centre of the caldera, in contrast with the previously recorded net gravity decreases (Rymer et al. 2010). The gravity increase is interpreted to correspond to a sub-surface mass increase of 0.68×10^{11} kg, at ~ 3 km depth. It may indicate the accumulation of fresh magma beneath the caldera, suggesting the onset of a new intrusion-eruption phase (Rymer et al. 2010). In July 2014, a landslide occurred in the south-eastern sector of the Öskjuvatn caldera and triggered a tsunami within the lake (Vogfjörd et al. 2015; Schöpa et al. 2016; Gylfadóttir et al. 2016).

Methodology

We focused on three main domains across the Askja central volcano: the Austurfjöll area, the Askja and the Öskjuvatn calderas (Figs. 1 and 2). Because of logistics and time limitations, our field observations and measurements within Austurfjöll were confined to the inner ~ 10 km^2 of the ~ 45 km^2 area of this massif, with field work taking place in
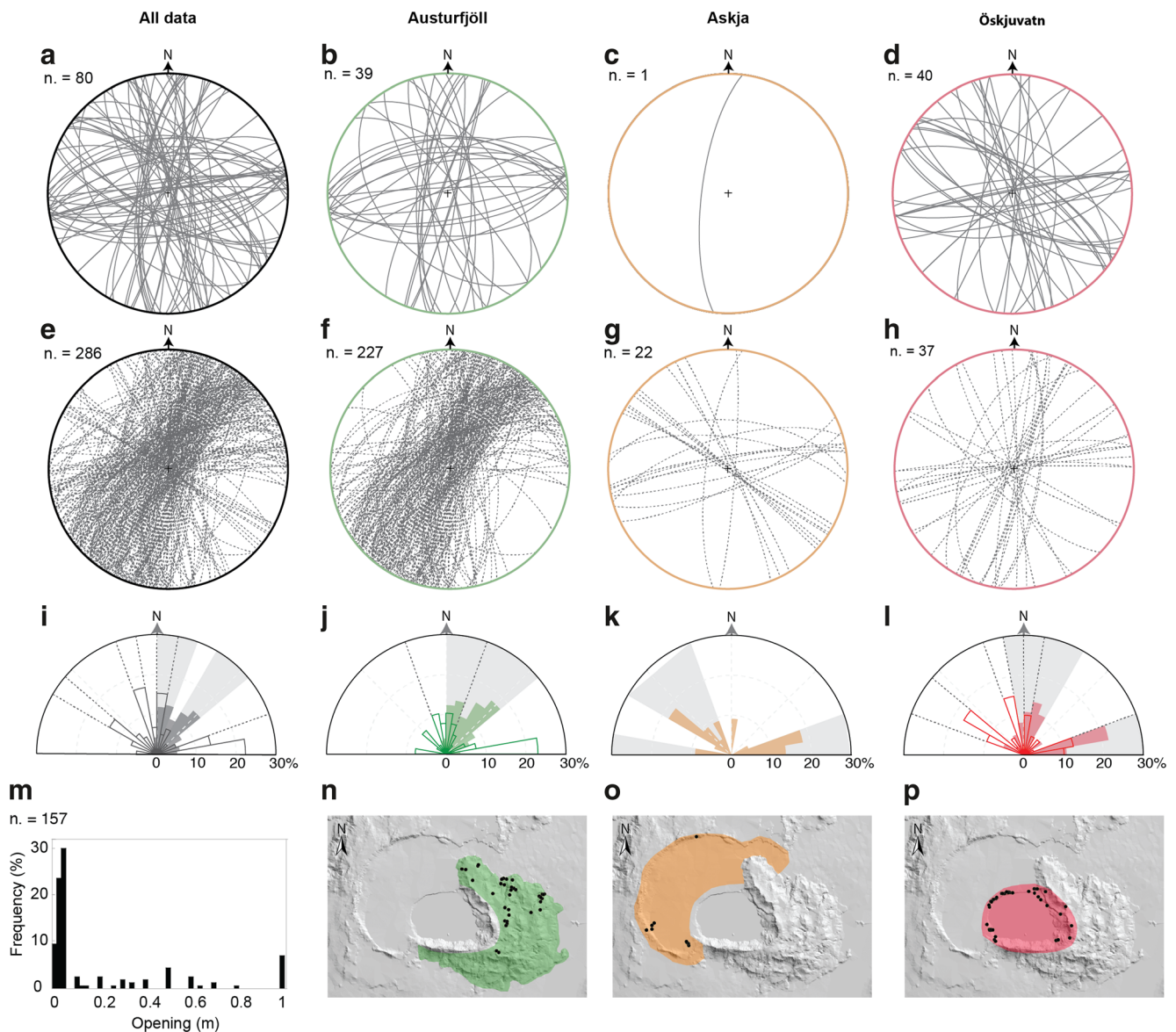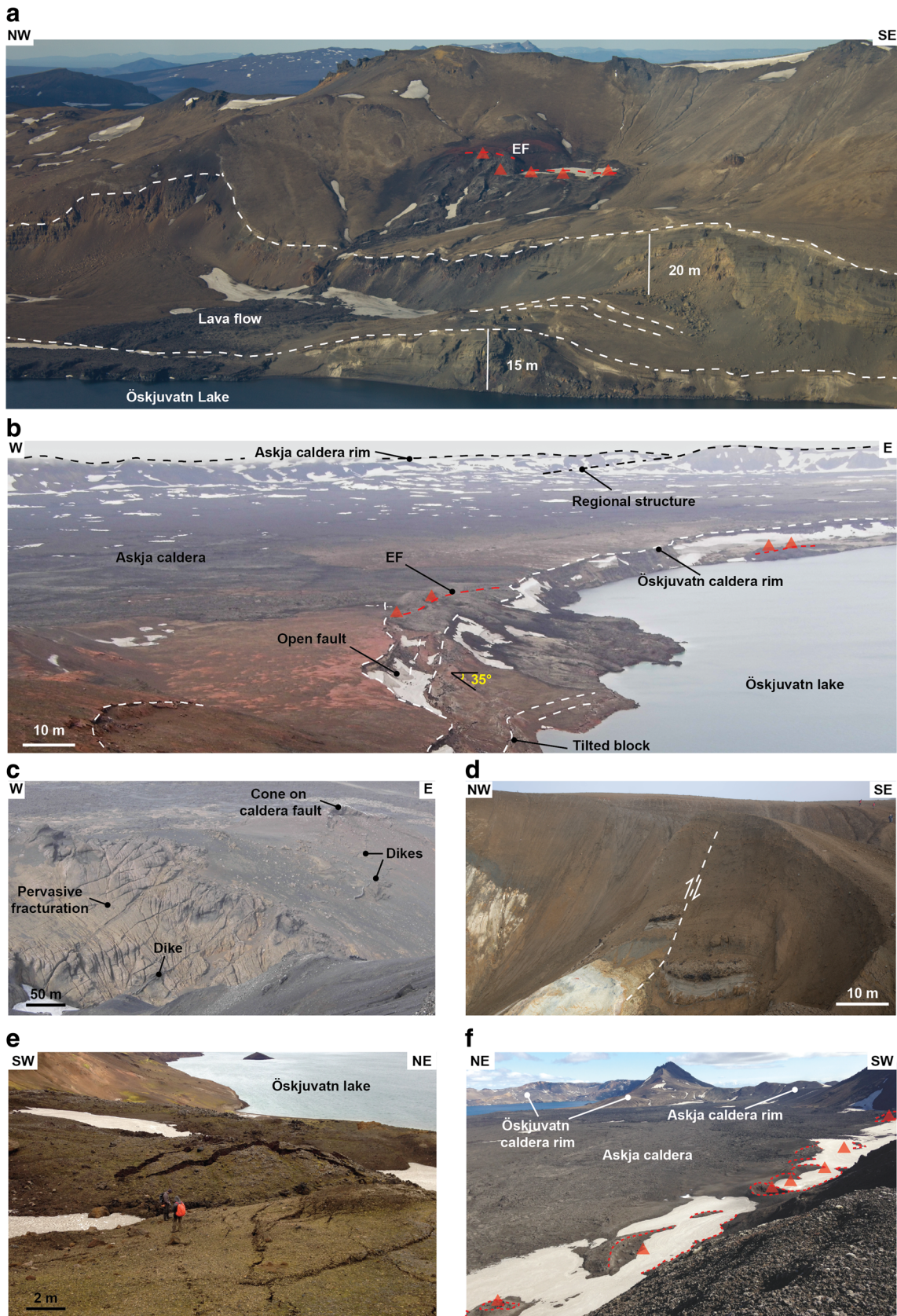
Fig. 3 Results of faults and tension fracture distribution analysis. Stereo-plots (on lower-hemisphere equal-area projections) show the orientation of faults planes within **a** the whole investigated area, **b** Austurfjöll, **c** Askja caldera and **d** Öskjuvatn caldera. Stereo-plots show the orientation of tension fractures planes within **e** the whole investigated area, **f** Austurfjöll, **g** Askja caldera and **h** Öskjuvatn caldera. Rose diagrams show the orientation of both faults (not filled) and tension fractures (colour filled) within **i** the whole investigated area, **j** Austurfjöll, **k** Askja caldera and **l** Öskjuvatn caldera. In the rose diagrams, the main clusters mentioned in the text are delimited with solid light grey line for tension fractures and with dashed lines for faults. **m** Histogram of tension fracture opening within the whole investigated area. **n–p** Sites of measurements (black dots) within Austurfjöll (green), Askja (orange) and Öskjuvatn (red) caldera areas. *n*, number of measurements

August 2012 and 2013. Within the three areas, we collected field data for faults (direction, dip and displacement), tension fractures (direction, dip, opening), dikes (direction, dip, thickness) and eruptive fissures (crater row direction). In total, we collected ~ 548 field measurements, of which 286 were related to tension fractures, 80 to faults, 160 to dikes and 22 to eruptive fissures. In Fig. 2, the field data are plotted on lower-hemisphere equal-area projections (using Stereonet 9 software; Allmendinger et al. 2012; Cardozo and Allmendinger 2013), where we have grouped our data into 17 measurement sites.

We supported our field observations with a remote sensing analysis. To do this, we manually mapped volcanic vents, eruptive fissures and lineaments using Google Earth (i.e. Spot Images from 2012 with a pixel size of 2.5 m), along with selected, cloud-free, ASTER (Advanced Spaceborne Thermal Emission and Reflection Radiometer) images (in particular, VNIR—visible and near-infrared images with 15 m pixels) and a digital elevation model (obtained from the interpolation of the topographic map with ~ 20-m spaced contours provided by the National Land Survey of Iceland and available at http://www.lmi.is/en).

a

NW

SE

EF

20 m

Lava flow

15 m

Öskjuvatn Lake

b

W

E

Askja caldera rim

Regional structure

Askja caldera

EF

Öskjuvatn caldera rim

Open fault

35°

Öskjuvatn lake

10 m

Tilted block

c

W

E

Cone on
caldera fault

Dikes

Pervasive
fracturation

Dike

50 m

d

NW

SE

10 m

e

SW

NE

Öskjuvatn lake

2 m

f

NE

SW

Öskjuvatn
caldera rim

Askja caldera rim

Askja caldera

◀ **Fig. 4** Examples of volcano-tectonic features at Askja; the location of each photo is indicated in Fig. 2. **a** View of Öskjuvatn caldera ring faults (white dashed line) with throws of 15–20 m in the area of the 1921 Bátshraun eruption (site 6 in Fig. 2). Red dashed line and triangles indicate the probable trace of the 1921 eruptive fissure—EF—and the vent locations. **b** View of the western Öskjuvatn caldera rim (site 13, Fig. 2) showing a major ring fault (white dashed line) which is partially intruded by a dike feeding an eruptive fissure (red dashed line and triangles). **c** View of the pre-Holocene succession in the Austurfjöll area (site 2, Fig. 2) showing NE-SW-oriented dikes (30–40 cm thick and 200–300 m long) intruding the highly fractured sub-glacial host rocks. **d** Normal fault (white dashed line) inside the Viti crater (site 6 in Fig. 2). **e** Open tension fractures parallel to the Öskjuvatn caldera rim observed during the 2013 field survey at the site of the 2014 landslide (site 10, Fig. 2). **f** Eruptive fissure along the Askja western caldera rim (site 15; Fig. 2); remnant crater rims are highlighted with a red dashed line, and red triangles indicate the centre of the crater

The remote sensing technique allowed us to quantify the distribution of volcanic vents within and around the Askja volcanic complex mapping volcanic vents with diameters > 5 m and then creating a vent density map.

We also examined the possible elongation and preferred orientation of the three calderas (Kollur, Askja and Öskjuvatn) by determining the shape of their outlines using both remote sensing data and previous studies. Caldera elongation is determined by its elliptical eccentricity (e) or $e = \frac{c}{a}$ where $c = \sqrt{a^2 - b^2}$; a and b are the length of the major and minor ellipse semi-axis; when $e = 0$, the ellipse becomes a circle.

Field measurements and remote sensing analysis

Brittle structures (faults and tension fractures) and dikes measured in Austurfjöll mainly affect hyaloclastite deposits with well-compacted ash and lapilli tuff, along with breccias and, more rarely, pillow lavas (Graettinger et al. 2013). In the Askja and Öskjuvatn calderas, the brittle structures affect lava flows and welded tuff deposits (Carey et al. 2008a, b), pyroclastic surges, fall deposits and phreatoplinian ash, all associated with the 1875 eruption (Carey et al. 2010).

Faults

We performed 80 measurements on faults, representing 22% of our total dataset for brittle structures. Among these 80 measurements, 39 are within Austurfjöll, 40 are along the rim of the Öskjuvatn caldera and one is located on the northwest rim of the Askja caldera (location of each fault is given in Fig. 2).

The stereo-plots and rose diagrams of Fig. 3, which display the entire fault dataset, show a scatter of directions, but with four clusters. These clusters are oriented N 80° E ± 10° (26% of the data), N 15° W ± 5° (12%), N 05° E ± 5° (11%) and N

55° W ± 5° (10%) (Fig. 3a, b). The fault kinematics, obtained from morphologic evidence (e.g. fault steps) and stratigraphic correlations, are consistently normal (dip slip component). The mean fault dip is 75°. At a few sites, such as along the main normal fault of the Öskjuvatn caldera (Fig. 4a), we found kinematic indicators (striations), showing a dominantly dip slip motion. However, these striations are rare, due to the poor consolidation of the pyroclastic products. About 25% of the faults are associated or close (< 30 m) to dikes or eruptive fissures, and have a comparable orientation with < 30° of deviation. Examples of this have been observed along Öskjuvatn at site 13 (Figs. 2 and 4b), in Austurfjöll at site 2 (Figs. 2 and 4c) and along the Askja caldera rim at site 15 (Figs. 2 and 4f).

Faults in Austurfjöll cluster in a N 20° W to N 20° E (38% of Austurfjöll faults) and in a N 85° E ± 5° (23%) direction (Fig. 3b, j). Most of these faults (34 out of 39) show a normal displacement of < 1 m, and only five reach up 2 to 5 m.

Along the northern and southern Askja Caldera rim, we only detected one normal fault. This is located at site 17 (Fig. 2) and strikes N 187° (i.e. close to parallel to the regional fissure swarm) with a dip slip component of 1 m (Fig. 3c). The Öskjuvatn caldera is bordered by well-preserved normal faults with throws of up to 100 m. The largest throws (10–100 m, measured at sites 8 and 11 in Fig. 2) are associated with the collapse structure of the Öskjuvatn caldera (Figs. 4a and SM 1). One of the faults also reaches the Víti crater at site 6 (Figs. 2 and 4d). Consequently, all 40 fault orientations measured in the rim of the Öskjuvatn caldera reflect the caldera's sub-circular structure, where they span 90% of the half-circle/upper stereographic hemisphere (Fig. 3d, l). Four fault clusters can be identified at N 60° W ± 10° (27% of fault measurements in Öskjuvatn), N 80° E ± 10° (22%), N 15° W ± 5° (15%) and N 05° E ± 5° (10%) directions.

Tension fractures

The 286 tension fractures that were measured in the field (Fig. 3e–h) represent 78% of the measurements carried out on the brittle structures. Most of these (60%) fall within the N 0° to N 50° E directions, with two distinct clusters at N 30°–N 50° E (27%) and N 0–20° E (24%) (Fig. 3e, i). The mean dip is 77°, with opening usually being < 10 cm and rarely > 1 m (Fig. 3m). Openings of > 1 m are likely to be related to cracks that have been widened by erosion of unconsolidated fall deposits.

Of the 286 detected tension fractures, 227 are located within Austurfjöll (Fig. 3f). Their directions are primarily focused between N 0° and N 50° E (68% of Austurfjöll tension fractures), with a mean value of N 31° E (Fig. 3j). Another 22 tension fractures are observed along the rim of the Askja caldera, focusing along the E-W (N 80° E ± 10° and N 85° W ± 5°; 26% of Askja tension fractures) and NW-SE (N 40° W ± 20°; 25%) directions (Fig. 3g, k). The remaining 37 tension fractures are located along the rim of the Öskjuvatn caldera.

Most of these fractures cluster along N-S to NE-SW directions (N 10° W ± 20°; 43% Öskjuvatn tension fractures) and along the N 80° E ± 10° direction (32%; Fig. 3h, l).

Tension fractures were also observed in correspondence to an active landslide affecting the 1875 eruption deposits in the south-eastern sector of the Öskjuvatn caldera (Fig. 4e). These observations were made 1 year before the same landslide underwent to a rapid sliding event on 21 July 2014. The estimated volume of the sliding event was 15–20 million m^3 with the landslide front that reached the bottom of Öskjuvatn lake with a consequent tsunami. Slow movement of the bedrock with an increase of velocity was detected since the summer of 2014 (Vogfjörd et al. 2015; Schöpa et al. 2016; Gylfadóttir et al. 2016).

Dikes, eruptive fissures and vent distribution

A total of 160 dikes and 22 eruptive fissures were measured in the field. Most of the dikes (48%) ranged from N 10° E to N 40° E in direction (Fig. 5a, b). The mean dip was 75°, with thicknesses commonly between 40 and 90 cm (60% of data; Fig. 5i). To further characterise the dike distribution, we also considered dike thickness as a function of dike azimuth direction: dikes thinner than 1 m can have any azimuth range, although with a peak between N 0° and N 50° E. Thicker dikes (> 1 m) range between the N 10° E and N 50° E directions (Fig. 5j).

Within Austurfjöll, we measured 117 dike orientations. These were mainly (51% of Austurfjöll dikes) confined to a NNE-SSW trend (N 10° E to N 40° W), with a mean dip of 74° (Fig. 5c, d). These dikes were frequently associated with pervasive fracturing of the hyaloclastite and were oriented parallel to, or intruded major tension fractures (Fig. 4c; e.g. site 1 and site 2 in Fig. 2). We also observed hyaloclastic dikes, these being fractures filled by thin hyaloclastic deposits. Their thickness is generally less than 10 cm (Graettinger et al. 2012), and the orientation is consistent with that of other dikes and brittle structures.

Along the Askja caldera rim, we observed 17 dikes. Most of these (82%; Fig. 5e, f) are exposed in the northern caldera wall and strike N 25° E ± 15°, with a mean dip of 81° (sites 1 and 17 in Fig. 2). Finally, 26 dikes were measured along the rim of the Öskjuvatn caldera. Although these were scattered in terms of orientation, half were NW-SE oriented (between N 20° W and N 50° W) and 20% were N-S oriented (N 0° ± 10°), with a mean dip of 78° (Fig. 5g, h).

The eruptive fissures observed in the field (minimum length of 100 m) revealed rather diverse orientations (Fig. 5a, b). However, the most common directions were N 30° E ± 10° (27% of eruptive fissures) and N 15° W ± 15° (32%). Nine eruptive fissures identified as having scattered orientations lie along the Askja caldera rim (Fig. 5e). They follow the strike of the rim or are perpendicular to it, as seen along the

western and south-western Askja caldera rim at sites 15 and 16 (Figs. 2 and 4f). This observation is also consistent with the ones of Hjartardóttir et al. (2009) and Hartley and Thordarson (2012). Within the Öskjuvatn caldera, 11 eruptive fissures were recognised, usually along the ring faults (Fig. 4a, b). Their orientations were dispersed and commonly consistent with those of the nearby dikes (Fig. 5g, h). In fact, most dikes and fissures (~ 75%) around the Öskjuvatn caldera were nearly circumferential (α > 50°; Fig. 5k) and followed the caldera rim (e.g. Fig. SM 1d).

To better characterise the overall dike plunges and their relations with major faults, we created a map of the dike poles' contours (Fig. 6). To do this, the dike outcrops were divided into six major groups, labelled 1 to 6 on Fig. 6. Despite dike dips being commonly > 70°, group 1 shows NNE-SSW trending dikes plunging eastward, whereas dikes of groups 2 and 4 have a westward plunge. Group 3 dikes, cropping out along the northeast margins of Austurfjöll, show a more different plunge, being towards the NW and SE. Within Öskjuvatn, caldera (groups 5 and 6) dikes dip inward, with azimuths parallel to the main caldera ring faults (Fig. 6).

By using remote sensing, we identified a total of 1800 vents. The ~ 80% of these lie outside of the central volcano, forming NNE-SSW-oriented cone rows up to 10 km long, both north and south of the volcano. Within the Austurfjöll area, the vent systems form clusters with an overall NNE-SSW trend, similar to the regional tectonic fabric (Fig. 7). However, there are also vent systems along the northern margin of Austurfjöll that run parallel with the southern margins of Öskjuop and define an overall WNW-ESE orientation. Both NNE-SSW and WNW-ESE trends are sub-parallel to the lineaments identified by Hartley and Thordarson (2012) (Fig. 1b).

To the west of Austurfjöll, vents and cone rows are mainly located along the Askja caldera rim and, to a lesser extent, along the Öskjuvatn caldera rim where most of the recent magmatic activity has taken place. Additionally, vents are also located in the Kollur caldera and in the area just north of it.

Like the vents and cone rows, dikes are also observed along the ring faults of the Öskjuvatn caldera (Fig. SM 1d), whereas the dikes located within Austurfjöll are confined to two NE-SW trending swarms. However, dike distribution analysis is strongly dependent on the extent of our field survey which does not encompass the Norður- and Vesturfjöll areas. In addition, the emplacement of the most recent lava flows has covered a large part of the Askja caldera floor limiting, or covering, potential exposure.

Regional lineaments, caldera rim and caldera shapes

The continuity of the western rim of the Askja caldera is disrupted by several NNE-SSW trending regional lineaments (Fig. 8a), which are associated with regional tectonic
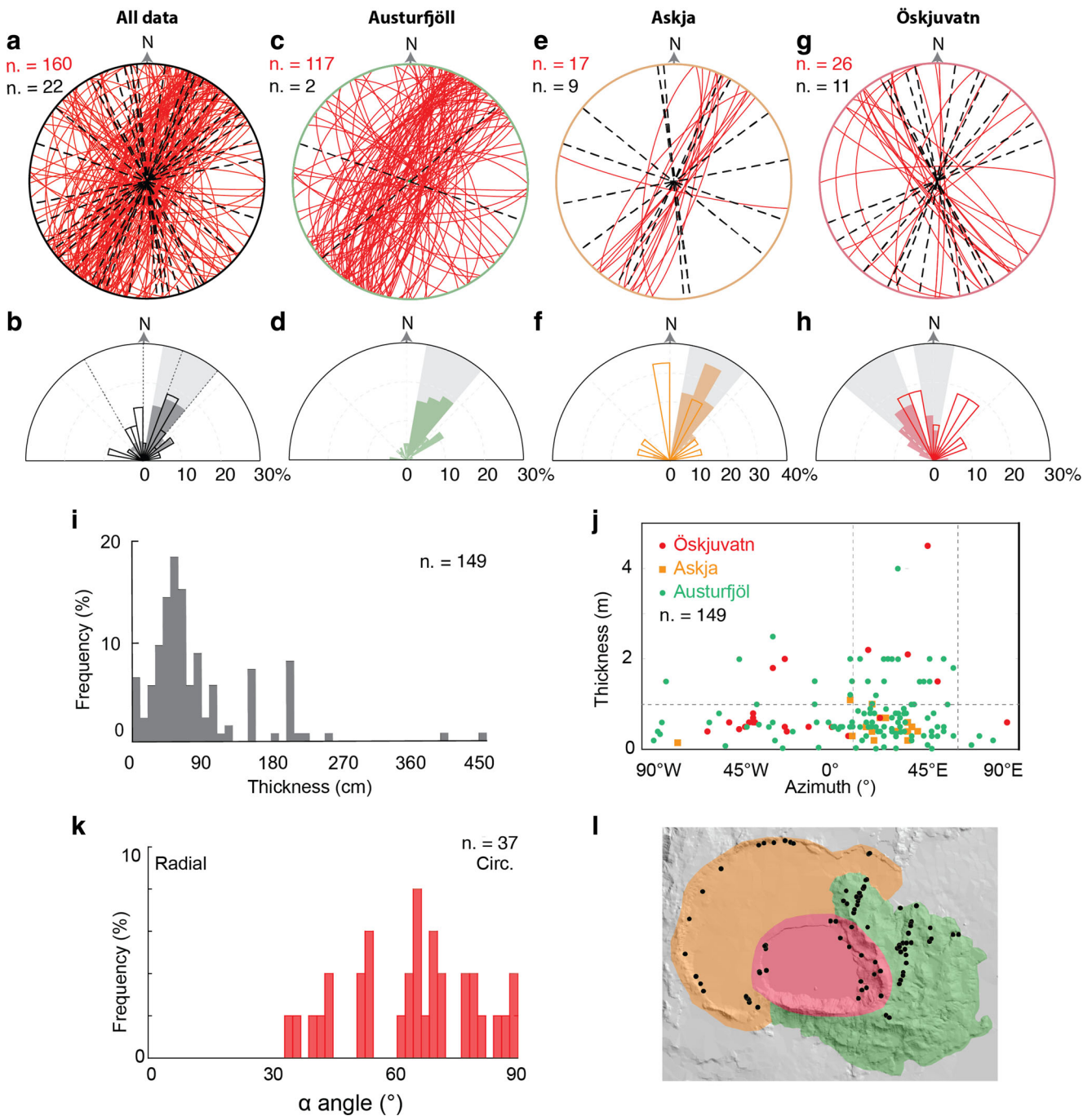
Fig. 5 Results of dike and eruptive fissures (EF) distribution analysis within **a** and **b** the whole investigated area, **c** and **d** Austurfjöll, **e** and **f** Askja caldera and **g** and **h** Öskjuvatn caldera. In the stereo-plot, dike planes are indicated with a solid red line and eruptive fissures are marked with a dashed black line. In rose diagrams, dike bars are filled whereas EF bars are not filled. The main clusters mentioned in the text are highlighted with solid light grey lines for dikes and with dashed lines for EF. **i** Histogram showing the frequency (in %) of dike thicknesses and **j** scatter diagram of dike thickness versus azimuth. Thresholds of 1 m for thickness and N 10° E–N 50° E for azimuths are indicated with grey dashed lines. **k** Histogram showing the frequency of the α angles for dikes and EF within the Öskjuvatn caldera (α is the angle between the direction connecting the magmatic feature to the caldera centre and the orientation of magmatic feature; if $\alpha = 0°$, the magmatic feature is radial with respect to the caldera; whereas if $\alpha = 90°$, the magmatic feature is circumferential (circ.)). **l** Sites of measurements (black dots)

structures (large eroded faults), cone rows and eruptive fissures (Hjartardóttir et al. 2009; Hartley and Thordarson 2012). We have identified six locations where the lineaments of the regional fissure swarm (hereafter termed regional lineaments) interact with the structures of the Askja caldera rim. At these locations, the angle between the regional lineaments and the caldera rim (i.e. the strike difference) can be measured. At locations 1, 2, 3, 5 and 6, the regional lineaments
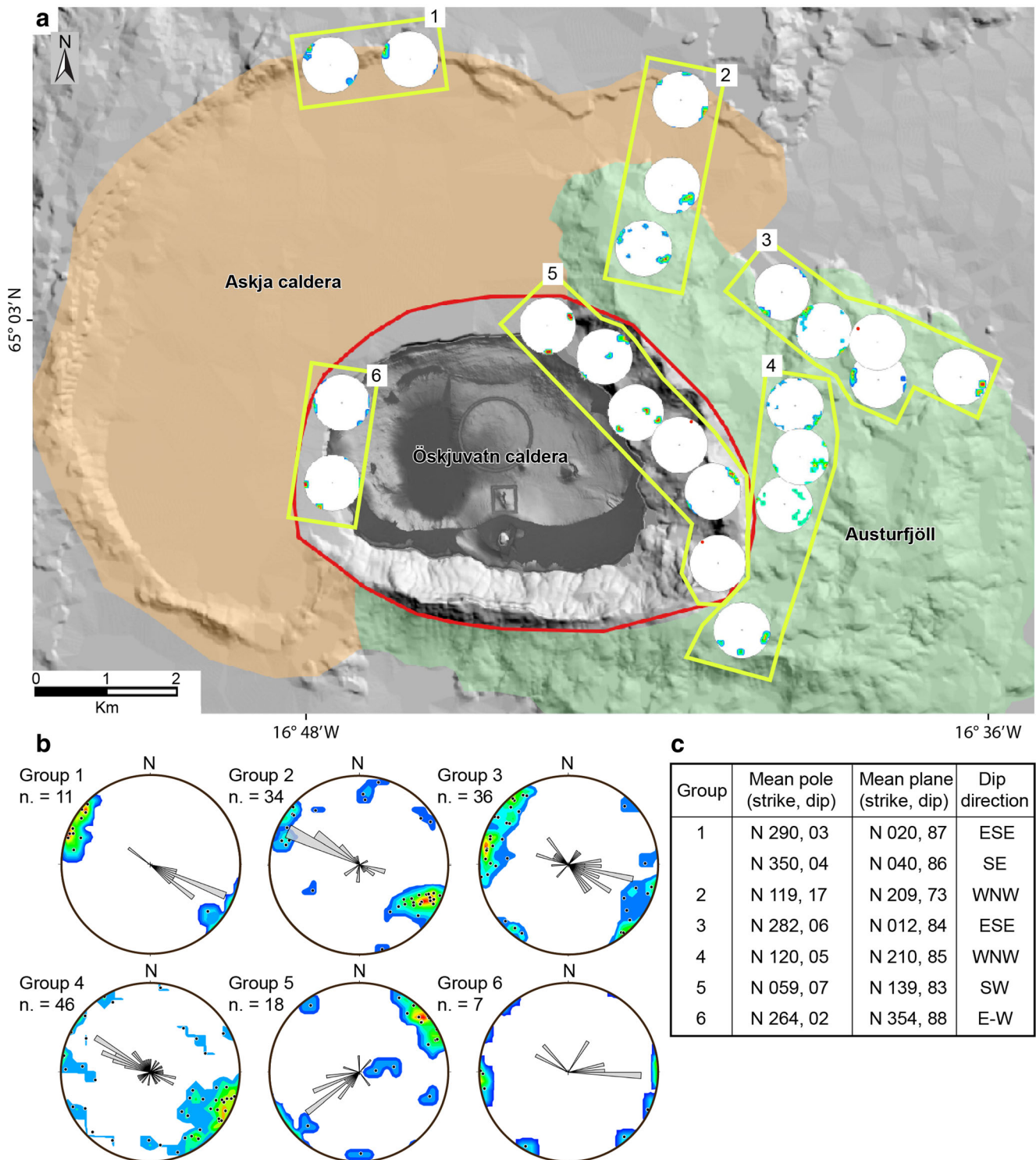
Fig. 6 a Stereonet-plots showing concentration of dike poles via density contours (contour lines are 2% spaced). The Öskjuvatn caldera area is highlighted by the red line and contains the bathymetric map of Fridriksson (2014); Askja caldera is shaded in light orange, while the pre-Holocene succession of Austurfjöll is shaded green. Stereo-plots obtained from multiple sites (yellow boxes) are divided into six major groups. The rainbow colours have been used to contour the pole densities: red identifies the highest (> 10%) and blue the lowest (2%) pole density. **b** Dike pole concentration for each of the six major groups overlain by a rose diagram showing dike dip directions. The bin size of the rose diagram is 5°; the length of each bin is proportional to the number of measurements (given us frequency in %); the plot radius corresponds to 15% of frequency for groups 2, 3 and 4 and to 30% of frequency for groups 1, 5 and 6. **c** Summary of the mean pole direction and the related mean plane and dip direction, for each group
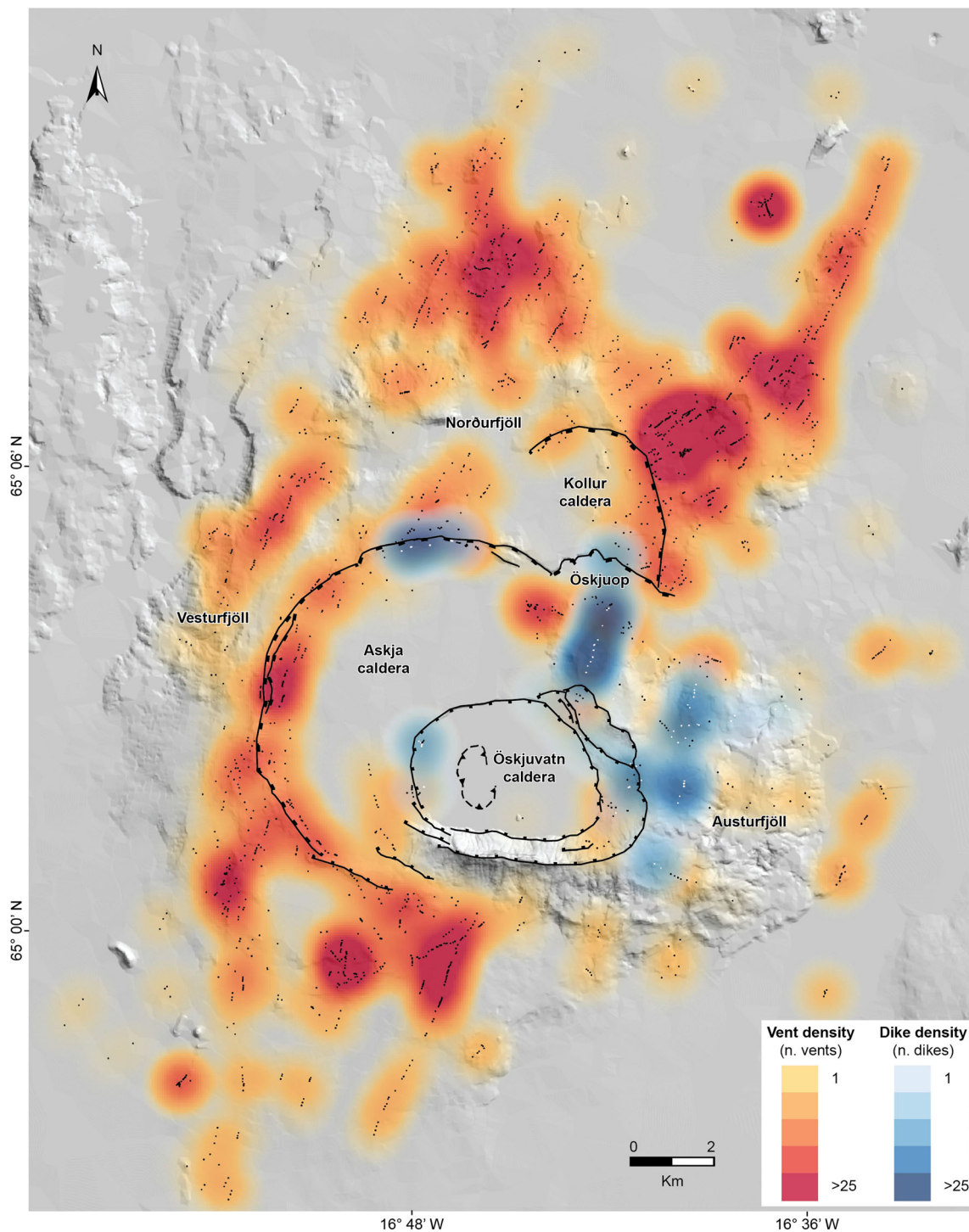
Fig. 7 Density map of vents (red) and dikes (blue). The point density has been obtained using the "heat map" function of Q-Gis; dike and vent datasets are analysed separately. Colour value for each pixel represents the number of vents (or dikes) within a radius of 900 m from that pixel. Vent and dike outcrops are represented with black and white dots, respectively. The ring and major intra-caldera faults are highlighted (dashed when inferred)

intersect and cross the caldera rim at angles ranging from 20° to 50° (Fig. 8a). The continuation of these regional lineaments across the caldera can also be observed, where these regional lineaments can be traced on Askja's caldera floor, even if their traces are less evident due to the cover by recent volcanic deposits (Fig. 8a).

From east to west, the angle between the regional lineaments and the caldera rim gradually decreases to 20° west of
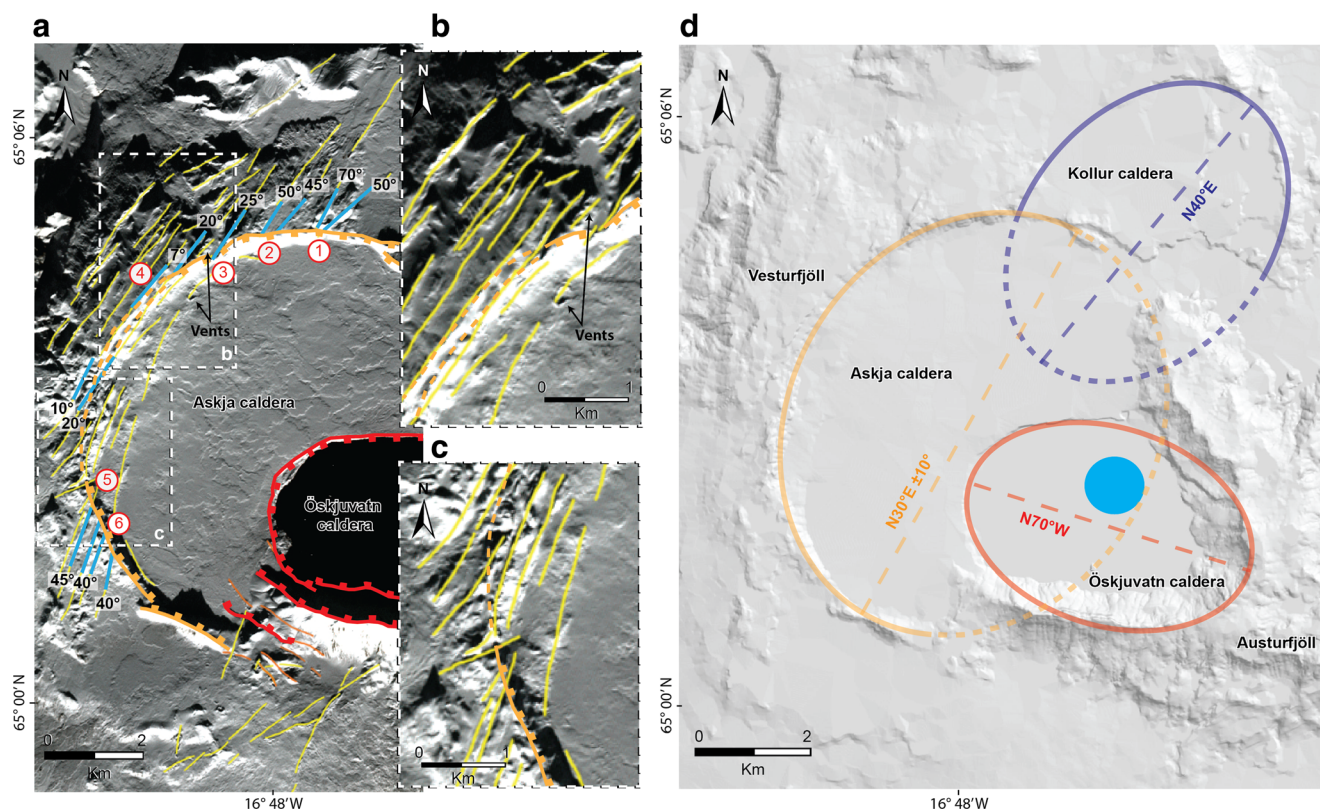
Fig. 8 **a** Map of major structures along the Askja caldera rim. Fissure-swarm-oriented lineaments are in yellow, caldera-rim-parallel structures are in light brown, Askja caldera rim is in orange (dashed when inferred) and Öskjuvatn caldera rim and related major faults are in red. Angles (black numbers) between the Askja caldera rim and the fissure swarms have been measured in correspondence to the pale blue lines. Red numbers mark the locations described in the text; **b** and **c** zoom of north-western and south-western Askja caldera rims, respectively (see

(**a**) for location). Fissure-swarm-oriented lineaments are in yellow, and caldera rim is in orange (dashed when inferred); **d** Ellipses and related major axis approximating the shape of Kollur (blue), Askja (orange) and Öskjuvatn (red) calderas. Ellipses are dashed when inferred. The smaller Sò lake that formed before Öskjuvatn caldera is highlighted in pale blue (from Fridriksson 2014). The ellipse defining the shape of Askja caldera is obtained by comparing previous published maps (Gudmundsson 1998; Hartley and Thordarson 2012) with modern images (see text for details)

locations 3 and 5 (Fig. 8a). Here, the caldera rim becomes less well defined (Fig. 8b). Further to the west (location 4), at the westernmost border of Askja, the lineaments and the caldera rim have a strike difference of ≤ 10°. Here, regional lineaments merge with the caldera rim (e.g. as at location 4 in Fig. 8a, b). While 20° is the lowest strike difference observed between the caldera rim and the lineaments crossing it, 10° is the highest observed strike difference between the caldera rim and the lineaments merging with it.

Ellipse tracing of the Kollur caldera allows its shape to be extrapolated from the remnant portion of the northern caldera ring fault. This ellipse, with an eccentricity of 0.66, is N 40° E oriented (Fig. 8d). This reconstruction is slightly different from that of Thorarinsson (1963, in Gudmundsson 1998) where it is suggested a possible NW-SE elongation of Kollur Caldera (N 50° W oriented). The shape of the Askja caldera can be reconstructed by following the remnant western caldera rim with remote sensing mapping, consulting the map of Thorarinsson (1963) in Gudmundsson (1998) or referring to the map drawn during the onset of Öskjuvatn caldera formation in 1876 (by Johnstrup 1877, in Hartley and Thordarson

2012). Using these sources, we find that the Askja caldera is elongated towards N 30° E ± 10° with an eccentricity of 0.5 ± 0.1. Caldera orientation is therefore roughly parallel to the trend of the fissure swarm immediately north of Askja. Conversely, the ellipse approximating the younger Öskjuvatn caldera is oriented ~ N 70° W, almost perpendicular to the other two calderas and to the fissure swarm. This is in agreement with Thorarinsson (1963) in Gudmundsson (1998). Its eccentricity is 0.74 (Fig. 8d).

Discussion

### Influence of the Askja central volcano on faulting and magma propagation

To best visualise the whole field-derived dataset, we merged all the data into a single histogram while highlighting the data from the different sectors within the Askja central volcano (Fig. 9). We also constructed a new structural map (Fig. 10) by merging data from the fields for dikes, faults and tension

fractures, with the vent density and lineaments at Vesturfjöll derived from the remote sensing analysis. We also added the lineaments at Austurfjöll mapped by Hartley and Thordarson (2012).

Our analysis highlights a difference in the orientation and frequency of the tectonic and magmatic features between the Austurfjöll area and the Öskjuvatn and Askja calderas (Fig. 9).

Austurfjöll, hosting only minor faults with throws usually < 5 m, has a volcano-tectonic pattern that is defined by a large number of N-S- to NE-SW-oriented tension fractures (68% of which are N 0° to N 50° E). These tension fractures have an orientation that partly overlaps with those of the faults (Fig. 3j) and dikes (51% of which are N 10° E to N 40° E, Figs. 5d and 7). In this sector, the main trend of the brittle deformation (faults and tension fractures) and magmatic features (dikes and eruptive fissures) is thus NNE-SSW (mainly N 10° E to N 40° E; Fig. 9). Only a small number of volcano-tectonic features having a WNW-ESE orientation have been observed. These are located in the northern sector of Austurfjöll where a fault cluster with an orientation of N 85° E ± 5° (Fig. 3j) and the vent pattern (Fig. 7) are parallel to the WNW-ESE volcano-tectonic lineaments identified by Hartley and Thordarson (2012) (Fig. 10). Therefore, we suggest that the NNE-SSW trending deformation measured in the field at Austurfjöll is related to the regional fissure swarm that controls a significant part of the development of the area. Local volcano-tectonic features oriented perpendicularly to the fissure swarm may overlap with the main deformation trend. The orientation of the local features may be constrained by a secondary structural pattern of unclear origin, although possibly induced by the overlap of calderas structures.

Conversely, Öskjuvatn and Askja calderas are both affected by large caldera ring faults, with throws of up to hundreds of meters (Figs. 4a, b and 10b). This represents the shallow portion of the ring fault systems. The youngest, Öskjuvatn caldera shows faults, tension fractures and eruptive fissures that are not well grouped having no major cluster with a preferred orientation (Figs. 3l and 5h). Although the dikes seem more focused, where there is a NW-SE- and NE-SW-oriented cluster, the overall orientation of the volcano-tectonic structures spans the whole azimuth range (Fig. 9), suggesting that the overall deformation pattern at Öskjuvatn follows the caldera rim pattern. Moreover, vents and dikes are mostly circumferential (Fig. 5k), located on the hanging-wall of the ring faults and dip towards the caldera centre (Figs. 4a, b, f, 6a and 10b). This suggests that most of the magmatic features observed at Öskjuvatn are the surface manifestation of dikes formed under the influence of the local stress field associated with a shallow magma chamber. This is in agreement with Gudmundsson (1998) and with
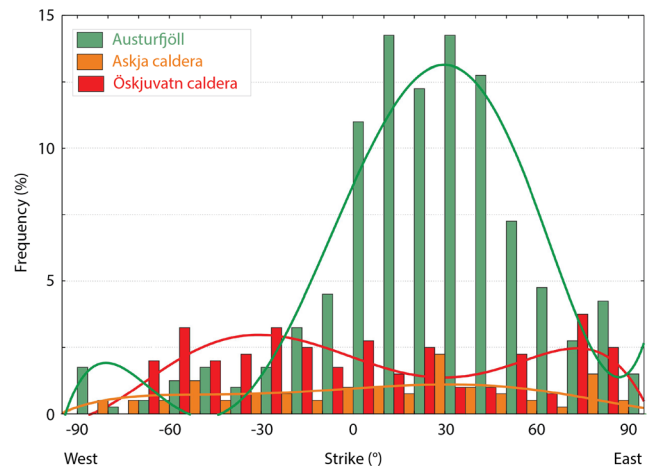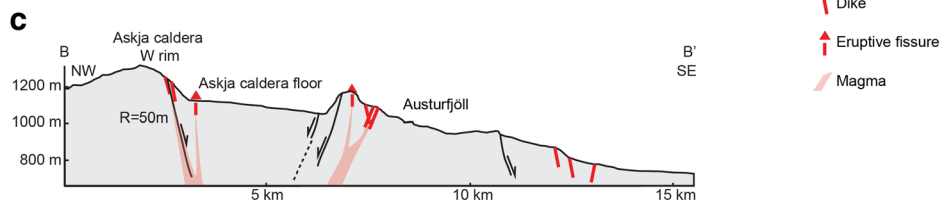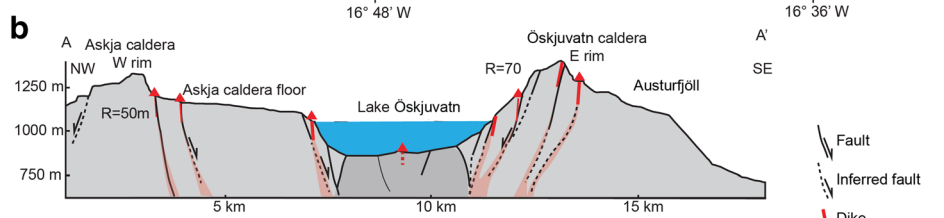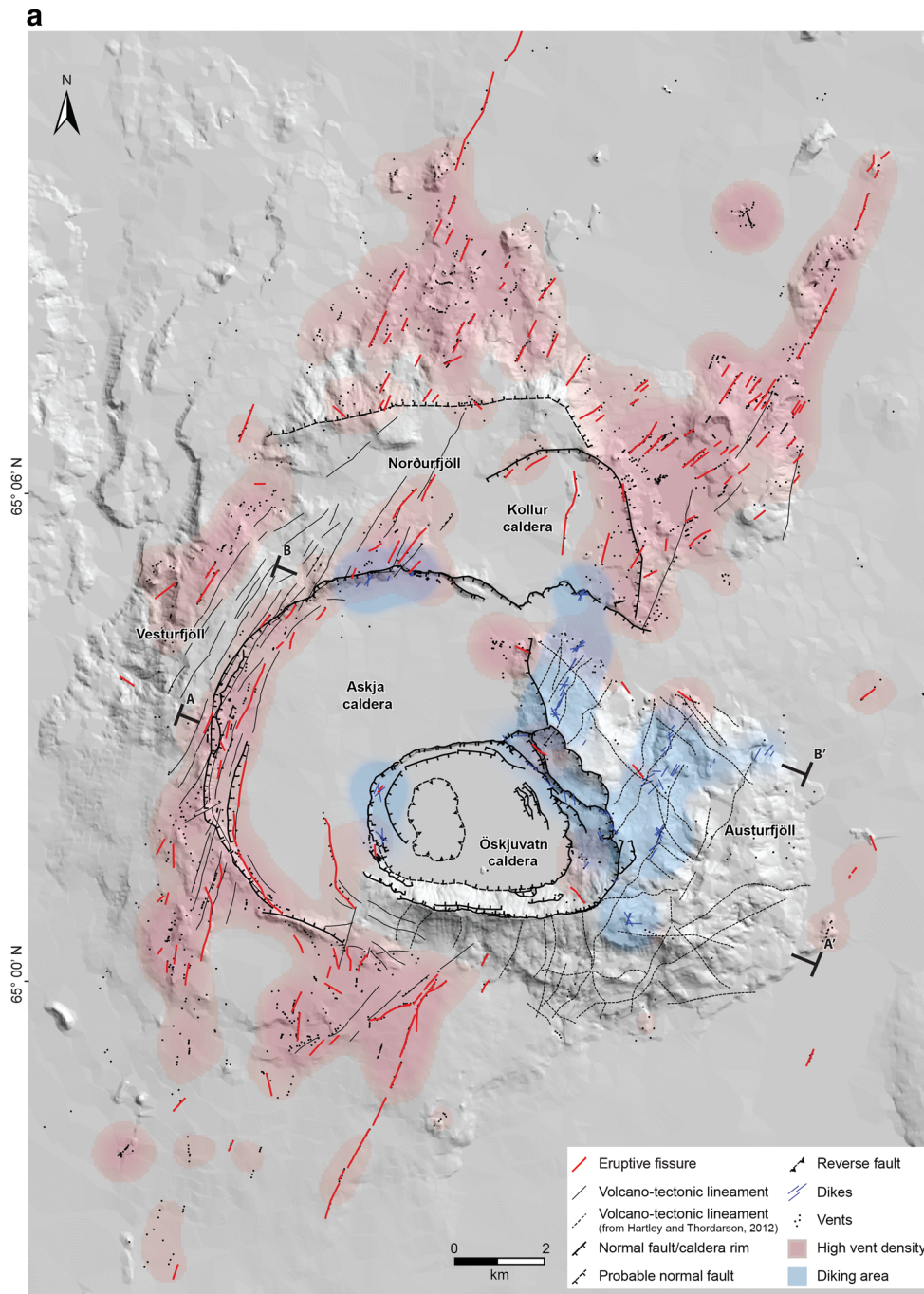

Fig. 9 Histogram showing the azimuth distribution of all structures (faults, dikes, tension fractures, eruptive fissures) measured in the field in Austurfjöll area, Askja and Öskjuvatn calderas

observations of extinct and eroded central volcanic complexes in Iceland (Gudmundsson 1995; Burchardt et al. 2013). In this context, the pre-existing caldera ring faults may be reactivated by magma intrusion, where the ring faults then control the path of the dikes feeding the circumferential fissures (Browning and Gudmundsson 2015). Indeed, most dikes and eruptive fissures at Öskjuvatn have been measured on the western, eastern and north-eastern caldera rims which are associated with caldera ring faults.

At the Askja caldera, we found evidence for a scattered pattern of structures (Fig. 9), suggesting a possible local influence on the caldera development, along with regional fissures that cross the caldera (Fig. 8a). Moreover, the high vent concentration along the western caldera fault (Fig. 7) and field evidence of eruptive fissures following the caldera rim (Fig. 4f) suggest that magmatic intrusions at the Askja caldera are partly controlled by the ring fault system (Fig. 10a, b). On the other hand, NE-trending eruptive fissures in western Askja (Fig. 10a) and field evidence of NE-SW-oriented dikes intruding the northwestern caldera wall (site 17 in Fig. 2; Fig. 5f) also suggest an influence of regional tectonic structures in determining the magma intrusion pattern.

The analysis of the interaction between the Askja caldera rim and the regional volcano-tectonic lineaments, interpreted as regional faults, suggests that their intersection angle controls the reactivation of the regional structures under a local stress field. If this angle is ≤ 10°, the local caldera faults may reactivate pre-existing regional faults (Figs. 8a and 10).

Outside of the calderas, linear volcanic vent systems form cone rows which are typically aligned along the regional fissure-swarm direction (NNE-SSW), suggesting that with an increase in distance from the central volcano, the magma migrates following the regional stress field (Fig. 10a).

a

Norðurfjöll

Kollur caldera

Vesturfjöll

B

A

Askja caldera

Öskjuvatn caldera

Austurfjöll

B′

A′

Eruptive fissure	Reverse fault
Volcano-tectonic lineament	Dikes
Volcano-tectonic lineament (from Hartley and Thordarson, 2012)	Vents
Normal fault/caldera rim	High vent density
Probable normal fault	Diking area

0   2
km

65° 06′ N

65° 00′ N

16° 48′ W

16° 36′ W

b

A   Askja caldera

NW   W rim

1250 m

R=50m

1000 m

750 m

Askja caldera floor

Lake Öskjuvatn

Öskjuvatn caldera

E rim   R=70

Austurfjöll

A′

SE

5 km   10 km   15 km

c

B   Askja caldera

NW   W rim

1200 m

R=50m

1000 m

800 m

Askja caldera floor

Austurfjöll

B′

SE

5 km   10 km   15 km

Fault
Inferred fault
Dike
Eruptive fissure
Magma

◀ **Fig. 10 a** Summary structural map of Askja central volcano showing the most important tectonic (regional and local) and magmatic features. Structures in Vesturfjöll are extracted from Fig. 8a, whereas structures in Austurfjöll are from Hartley and Thordarson (2012). Magmatic areas, indicated in red (vents) and pale blue (dikes), have been extracted from Fig. 7. Vent density has been filtered considering only pixels with five vents or more within in a radius of 900 m. Schematic and interpretative structural cross-sections along the lines **b** A–A′ and **c** B–B′ (locations in panel **a**). Caldera fault geometry at depth is based on analogue modelling of calderas (e.g. Acocella 2007), whereas the dip angle of regional normal faults is from Forslund and Gudmundsson (1992)

Our results show that local caldera structures, representing a possible preferential pathway to channelize magma up to the surface, become prominent in the central volcano where the local stress field dominates, while dikes outside the caldera system are controlled by the regional tectonics (Fig. 10a, b). Our results also suggest that the external portions of the Askja central volcano (i.e. Austurfjöll to the east and the Askja caldera rim to the west) developed under a partial influence of the regional tectonic stress field, being affected by the fissure-swarm-related deformation. Moreover, we highlight an overall coincidence in the location and trend of the magmatic features (dikes and vents) and the major caldera discontinuities (Figs. 4 and 10) and an overall dip of both regional (within Austurfjöll and along the northern Askja caldera rim) and local dikes towards the central portion of the volcano. This confirms that Askja lies in the middle of a rift system in which magma may follow the major fissure-swarm-related regional structures, generally dipping with a high angle (Fig. 10b, c).

Overall structure of the Askja central volcano

Several calderas at divergent plate boundaries show an elliptical planar shape with elongation parallel or, in most cases, perpendicular to the regional fissure swarm. While the former case applies to, for example, Erta Ale in Afar (Acocella 2006); the latter applies to Long Valley in California and Krafla in Iceland (Bosworth et al. 2003). In a similar fashion, the structure of the Askja central volcano suggests the presence of both rift-parallel and rift-perpendicular calderas. Our remote sensing analysis suggests that Kollur and Askja calderas (which are oriented N 30° E ± 10°) are likely parallel to the regional fissure swarm, whereas the younger Öskjuvatn caldera (which is oriented N 70° W) is almost perpendicular to the general pattern of the fissure swarm.

Several mechanisms, usually related to regional tectonics, have been proposed for the development of rift-parallel and rift-perpendicular calderas (Acocella 2007). For example, rift-parallel calderas may form above an elliptical magmatic chamber controlled by the influence of pre-existing rift structures as, for example, in the Kenya Rift (Bosworth et al. 2003). At Askja, the regional trending dikes, clustering at N 25° E ± 15° and intruding the northern Askja caldera rim (e.g. site 17

in Fig. 2), suggest that this caldera may be partly related to the development of a magmatic source controlled by regionally tectonics.

Rift-perpendicular calderas may be related to the interaction between the caldera ring faults and the fissure-swarm structures (Acocella et al. 2004) or to the elongation of the magma chamber parallel to the extension direction (Bosworth et al. 2003; Ruch and Walter 2010). These mechanisms may provide an explanation for the E-W elongation of the Öskjuvatn caldera. Additionally, the elongation of this caldera may have been enhanced by topographic effects, such as the collapse structures extending outwards into a zone of high relief. This process, enhanced by the topographic load, has been observed in analogue models (Belousov et al. 2005). This may explain the enlargement of the Öskjuvatn caldera towards the SE, into an area of higher topography represented by the Austurfjöll massif. Indeed, similarly to analogue models, the higher eastern rim of the Öskjuvatn caldera is characterised by a complex structure, with multiple overlapping normal faults showing the largest throws and extending outward towards the area of higher topography (sites 8 and 11 in Fig. 2; e.g. Fig. 4a). For this reason along with the presence of rock-alteration areas, landslides are more likely to occur within this sector of the volcano. Fractures observed in the area of the 2014 landslide, and the following sliding event, may be evidence of such an active gravitational process. The structural fabric of the Eastern Öskjuvatn contrasts markedly with that shown by a single continuous and regular ring fault along the lower and flat NW rim of the caldera (Fig. 2).

In addition, bathymetric data from the Öskjuvatn lake suggest that the Öskjuvatn caldera consists of two nested collapse structures: an outer one corresponding to the shore of the Öskjuvatn Lake, and an inner one located in the deeper centre of the lake (Figs.1 and 10a, b; Fridriksson 2014). These two nested collapse structures locally have a tilted area between them (e.g. site 13 in Figs. 2 and 4b) and their overall geometric configuration resembles that of the nested collapse observed in analogue models of caldera formation (Fig. 10b; Acocella 2007) as well as along fissure swarms (Trippanera et al. 2015). Therefore, we speculate that the Öskjuvatn caldera is a well-developed caldera formed by two nested ring structures.

Moreover, even though the precise relationships between Kollur and Askja calderas are not straightforward, the Askja caldera partially overlaps with the older southern Kollur rim. In addition, the central portion of the youngest Öskjuvatn coincides with the possible location of vents responsible for the 1875 eruption, which were apparently controlled by the location of the larger Askja caldera ring fault. Indeed, here the subsidence initiating the Öskjuvatn caldera started (Fig. 2; Carey et al. 2010; Hartley and Thordarson 2012; Fridriksson 2014). This spatial and temporal evolution of the three overlapping calderas in the Askja central volcano suggests an overall southward migration of the calderas which location

is influenced in turn by the pre-existing older caldera ring faults.

Askja central volcano in the frame of the Icelandic rift

Askja provides a case type example of a volcanic complex located on a rift zone and exhibiting both rift-parallel and rift-perpendicular structures. This feature, while already observed in continental rift zones (Acocella et al. 2002), is quite distinctive among rift zones in oceanic domains. In fact, along fast spreading ridges, the structures are systematically rift-parallel (Lagabrielle et al. 2001; Acocella 2014). At slow-spreading ridges, as at the Icelandic rift, rift-parallel structures still predominate, even though there is also evidence for rift-perpendicular structures. Examples of rift-perpendicular structures include the Krafla swarm to the north of Askja and, possibly, the Grímsvötn central volcano to the south. They are also common in the East Volcanic Zone at Hengill and on the Reykjanes Peninsula.

The Krafla swarm, for example, is affected by linear eruptive fissures parallel to the N-S trending regional deformation pattern (Björnsson et al. 1977; Tryggvason 1984; Saemundsson 1991) but in contrast to Askja, the rift-perpendicular Krafla caldera is strongly dissected by the regional faults along which volcanic activity predominates (Saemundsson 1991). This suggests that Krafla caldera is experiencing a stronger regional deformation compared to the local one induced by the caldera and its underlying magma chamber. This results in a greater control by regional tectonics than at Askja. Conversely, Grímsvötn is a central volcano without fissure swarms (only two volcanic fissures occurred outside the volcano in the last 9000 years), suggesting a minimum interaction with regional structures. Therefore, Askja appears to be a volcano with an intermediate influence of the regional fissure swarm among those observed along slow-spreading ridges, where the local and regional stress field are both present and balanced, unlike nearby Krafla to the north (related to predominant regional structures) and Grímsvötn to the south (related to predominant local structures). This is also compatible with the northward increase in the regional extension rate from Grímsvötn to Krafla (e.g. Perlt et al. 2008).

Conclusions

While some features of the Askja complex appear more controlled by regional tectonics (Austurfjöll and partly the western Askja border), others (part of Askja and the Öskjuvatn calderas) appear controlled by a local stress field induced by the local magma plumbing system and the related caldera ring fault structures. Our data highlight an overall interaction between the regional rift structures and the local caldera structures suggesting that regional structures are reactivated during caldera collapse. In addition, the volcano is characterised by rift-parallel and rift-perpendicular overlapping caldera structures whose location depends on their temporal evolution. Overall, Askja seems to show an intermediate behaviour between Krafla and Grímsvötn, with the most balanced amount of local and regional control on the magmatic and tectonic features. Indeed, Askja, Krafla and Grímsvötn seem to be characterised by a marked northward increase in the influence of the regional structures, passing from a mostly local to a predominantly regional stress control. This may result from the northward increase in the amount of extension, from a few millimetres per year to > 20 mm/year (e.g. Perlt et al. 2008), confirming the importance of the plate spreading rate in shaping divergent plate boundaries (Acocella 2014).

References

Acocella V (2006) Regional and local tectonics at Erta Ale caldera, Afar (Ethiopia). J Struct Geol 28(10):1808–1820. https://doi.org/10.1016/j.jsg.2006.06.014

Acocella V (2007) Understanding caldera structure and development: an overview of analogue models compared to natural calderas. Earth Sci Rev 85(3-4):125–160. https://doi.org/10.1016/j.earscirev.2007.08.004

Acocella V (2014) Structural control on magmatism along divergent and convergent plate boundaries: overview, model, problems. Earth Sci Rev 136:226–288. https://doi.org/10.1016/j.earscirev.2014.05.006

Acocella V, Trippanera D (2016) How diking affects the tectonomagmatic evolution of slow spreading plate boundaries: overview and model. Geosphere 12:GES01271.1. https://doi.org/10.1130/GES01271.1

Acocella V, Korme T, Salvini F, Funiciello R (2002) Elliptic calderas in the Ethiopian Rift: control of pre-existing structures. J Volcanol Geotherm Res 119(1-4):189–203. https://doi.org/10.1016/S0377-0273(02)00342-6

Acocella V, Korme T, Salvini F (2003) Formation of normal faults along the axial zone of the Ethiopian Rift. J Struct Geol 25(4):503–513. https://doi.org/10.1016/S0191-8141(02)00047-0

Acocella V, Funiciello R, Marotta E, Orsi G, de Vita S (2004) The role of extensional structures on experimental calderas and resurgence. J Volcanol Geotherm Res 129(1-3):199–217. https://doi.org/10.1016/S0377-0273(03)00240-3

Allmendinger RW, Cardozo N, Fisher D (2012) Structural geology algorithms: vectors and tensors in structural geology. Cambridge University Press, Cambridge

Andrew REB, Gudmundsson A (2008) Volcanoes as elastic inclusions: their effects on the propagation of dykes, volcanic fissures, and volcanic zones in Iceland. J Volcanol Geotherm Res 177(4):1045–1054. https://doi.org/10.1016/j.jvolgeores.2008.07.025

Annertz K, Nilsson M, Sigvaldason GE (1985) The postglacial history of Dyngjufjoll

Belousov A, Walter TR, Troll VR (2005) Large-scale failures on domes and stratocones situated on caldera ring faults: sand-box modeling of natural examples from Kamchatka, Russia. Bull Volcanol 67(5): 457–468. https://doi.org/10.1007/s00445-004-0387-1

Björnsson A, Saemundsson K, Einarsson P et al (1977) Current rifting episode in north Iceland. Nature 268:495–500

Bosworth W, Burke K, Strecker M et al (2003) Effect of stress fields on magma chamber stability and the formation of collapse calderas. Tectonics 22(4):1–21. https://doi.org/10.1029/2002TC001369

Brown GC, Everett SP, Rymer H, McGarvie DW, Foster I (1991) New light on caldera evolution—Askja, Iceland. Geology 19(4):352–355. https://doi.org/10.1130/0091-7613(1991)019<0352

Browning J, Gudmundsson A (2015) Caldera faults capture and deflect inclined sheets: an alternative mechanism of ring dike formation. Bull Volcanol 77(1):1–13. https://doi.org/10.1007/s00445-014-0889-4

Buck WR, Einarsson P, Brandsdòttir B (2006) Tectonic stress and magma chamber size as controls on dike propagation: constraints from the 1975-1984 Krafla rifting episode. J Geophys Res Solid Earth 111(B12):1–15. https://doi.org/10.1029/2005JB003879

Burchardt S, Troll VR, Mathieu L, Emeleus HC, Donaldson CH (2013) Ardnamurchan 3D cone-sheet architecture explained by a single elongate magma chamber. Sci Rep 3(1):1–7. https://doi.org/10.1038/srep02891

Cardozo N, Allmendinger RW (2013) Spherical projections with OSXStereonet. Comput Geosci Geosci 51:193–205. https://doi.org/10.1016/j.cageo.2012.07.021

Carey RJ, Houghton BF, Thordarson T (2008a) Contrasting styles of welding observed in the proximal Askja 1875 eruption deposits I: regional welding. J Volcanol Geotherm Res 171(1-2):1–19. https://doi.org/10.1016/j.jvolgeores.2007.11.020

Carey RJ, Houghton BF, Thordarson T (2008b) Contrasting styles of welding observed in the proximal Askja 1875 eruption deposits II: local welding. J Volcanol Geotherm Res 171(1-2):20–44. https://doi.org/10.1016/j.jvolgeores.2007.11.017

Carey RJ, Houghton BF, Thordarson T (2010) Tephra dispersal and eruption dynamics of wet and dry phases of the 1875 eruption of Askja volcano, Iceland. Bull Volcanol 72(3):259–278. https://doi.org/10.1007/s00445-009-0317-3

De Zeeuw-van Dalfsen E, Rymer H, Sigmundsson F, Sturkell E (2005) Net gravity decrease at Askja volcano, Iceland: constraints on processes responsible for continuous caldera deflation, 1988-2003. J Volcanol Geotherm Res 139(3-4):227–239. https://doi.org/10.1016/j.jvolgeores.2004.08.008

De Zeeuw-van Dalfsen E, Pedersen R, Hooper A, Sigmundsson F (2012) Subsidence of Askja caldera 2000-2009: Modelling of deformation processes at an extensional plate boundary, constrained by time series InSAR analysis. J Volcanol Geotherm Res 213–214:72–82. https://doi.org/10.1016/j.jvolgeores.2011.11.004

De Zeeuw-van Dalfsen E, Rymer H, Sturkell E et al (2013) Geodetic data shed light on ongoing caldera subsidence at Askja, Iceland. Bull Volcanol 75(5):1–13. https://doi.org/10.1007/s00445-013-0709-2

DeMets C, Gordon RG, Argus DF (2010) Geologically current plate motions. Geophys J Int 181(1):1–80. https://doi.org/10.1111/j.1365-246X.2009.04491.x

Ebinger C, Ayele A, Keir D, Rowland J, Yirgu G, Wright T, Belachew M, Hamling I (2010) Length and timescales of rift faulting and magma intrusion: the Afar rifting cycle from 2005 to present. Annu Rev Earth Planet Sci 38(1):439–466. https://doi.org/10.1146/annurev-earth-040809-152333

Forslund T, Gudmundsson A (1992) Structure of Tertiary and Pleistocene normal faults in Iceland. Tectonics 11(1):57–68. https://doi.org/10.1029/91TC01536

Fridriksson A (2014) What is below the water masses? Multibeam studies of Öskjuvatn, Thingvallavatn and Kleifarvatn. PhD thesis, University of Iceland, Faculty of Earth Sciences, 1–76

Gautneb H, Gudmundsson A (1992) Effect of local and regional stress-fields on sheet emplacement in West Iceland. J Volcanol Geotherm Res 51(4):339–356. https://doi.org/10.1016/0377-0273(92)90107-O

Graettinger AH, Skilling I, Mcgarvie D, Höskuldsson Á (2012) Intrusion of basalt into frozen sediments and generation of coherent-margined volcaniclastic dikes (CMVDs). J Volcanol Geotherm Res 217–218: 30–38. https://doi.org/10.1016/j.jvolgeores.2011.12.008

Graettinger AH, Skilling I, Mcgarvie D, Höskuldsson Á (2013) Subaqueous basaltic magmatic explosions trigger phreatomagmatism: a case study from Askja, Iceland. J Volcanol Geotherm Res 264:17–35. https://doi.org/10.1016/j.jvolgeores.2013.08.001

Greenfield T, White RS, Roecker SW (2016) The magmatic plumbing system of the Askja central volcano, Iceland, as imaged by seismic tomography. J Geophys Res Solid Earth 121(10):7211–7229. https://doi.org/10.1002/2016JB013163

Gudmundsson A (1995) Infrastructure and mechanics of volcanic systems in Iceland. J Volcanol Geotherm Res 64(1-2):1–22. https://doi.org/10.1016/0377-0273(95)92782-Q

Gudmundsson A (1998) Magma chambers modeled as cavities explain the formation of rift zone central volcanoes and their eruption and intrusion statistics. J Geophys Res 103:7401–7412. https://doi.org/10.1029/97JB03747

Gudmundsson A (2006) How local stresses control magma-chamber ruptures, dyke injections, and eruptions in composite volcanoes. Earth Sci Rev 79(1-2):1–31. https://doi.org/10.1016/j.earscirev.2006.06.006

Gudmundsson A (2011) Deflection of dykes into sills at discontinuities and magma-chamber formation. Tectonophysics 500(1-4):50–64. https://doi.org/10.1016/j.tecto.2009.10.015

Gudmundsson A, Andrew REB (2007) Mechanical interaction between active volcanoes in Iceland. Geophys Res Lett 34(10):1–5. https://doi.org/10.1029/2007GL029873

Gudmundsson Å, Backstrom K (1991) Structure and development of the Sveinagja graben, Northeast Iceland. Tectonophysics 200(1-3):111–125. https://doi.org/10.1016/0040-1951(91)90009-H

Gudmundsson A, Friese N, Andrew R et al (2009) Effects of dyke emplacement and plate pull on mechanical interaction between volcanic systems and central volcanoes in Iceland. Spec Publ IAVCEI 331–347

Gudmundsson A, Lecoeur N, Mohajeri N, Thordarson T (2014) Dike emplacement at Bardarbunga, Iceland, induces unusual stress changes, caldera deformation, and earthquakes. Bull Volcanol 76(10):1–7. https://doi.org/10.1007/s00445-014-0869-8

Gudmundsson MT, Jónsdóttir K, Hooper A, et al (2016) Gradual caldera collapse at Bárdarbunga volcano, Iceland, regulated by lateral magma outflow. Science (80-). https://doi.org/10.1126/science.aaf8988.sciencemag.org

Gylfadóttir SS, Kim J, Helgason JK, et al (2016) The 2014 Lake Askja rockslide tsunami – optimization of landslide parameters comparing numerical simulations with observed run-up

Hartley ME, Thordarson T (2012) Formation of Öskjuvatn caldera at Askja, North Iceland: mechanism of caldera collapse and implications for the lateral flow hypothesis. J Volcanol Geotherm Res 227–228:85–101. https://doi.org/10.1016/j.jvolgeores.2012.02.009

Hartley ME, Thordarson T (2013) The 1874-1876 volcano-tectonic episode at Askja, North Iceland: lateral flow revisited. Geochem Geophys Geosyst 14(7):2286–2309. https://doi.org/10.1002/ggge.20151

Hartley ME, Thordarson T, De Joux A (2016) Postglacial eruptive history of the Askja region, North Iceland. Bull Volcanol 78(4):1–18. https://doi.org/10.1007/s00445-016-1022-7

Hjartardóttir ÁR, Einarsson P (2015) The interaction of fissure swarms and monogenetic lava shields in the rift zones of Iceland. J Volcanol

Geotherm Res 299:91–102. https://doi.org/10.1016/j.jvolgeores.2015.04.001

Hjartardóttir ÁR, Einarsson P, Sigurdsson H (2009) The fissure swarm of the Askja volcanic system along the divergent plate boundary of N Iceland. Bull Volcanol 71(9):961–975. https://doi.org/10.1007/s00445-009-0282-x

Hjartardóttir ÁR, Einarsson P, Bjorgvinsdòttir SG (2016a) Fissure swarms and fracture systems within the Western Volcanic Zone, Iceland—effects of spreading rates. J Struct Geol 91:39–53. https://doi.org/10.1016/j.jsg.2016.08.007

Hjartardóttir ÁR, Einarsson P, Gudmundsson MT, Högnadóttir T (2016b) Fracture movements and graben subsidence during the 2014 Bárðarbunga dike intrusion in Iceland. J Volcanol Geotherm Res 310:242–252. https://doi.org/10.1016/j.jvolgeores.2015.12.002

Hollingsworth J, Leprince S, Ayoub F, Avouac JP (2012) Deformation during the 1975-1984 Krafla rifting crisis, NE Iceland, measured from historical optical imagery. J Geophys Res Solid Earth 117(B11):1–24. https://doi.org/10.1029/2012JB009140

Hollingsworth J, Leprince S, Ayoub F, Avouac JP (2013) New constraints on dike injection and fault slip during the 1975-1984 Krafla rift crisis, NE Iceland. J Geophys Res Solid Earth 118(7):3707–3727. https://doi.org/10.1002/jgrb.50223

Hreinsdottir S, Sigmundsson F, Roberts MJ et al (2014) Volcanic plume height correlated with magma-pressure change at Grimsvotn volcano, Iceland. Nat Geosci 7(3):214–218. https://doi.org/10.1038/ngeo2044

Hutchison W, Mather TA, Pyle DM, Biggs J, Yirgu G (2015) Structural controls on fluid pathways in an active rift system: a case study of the Aluto volcanic complex. Geosphere 11(3):542–562. https://doi.org/10.1130/GES01119.1

Hutchison W, Biggs J, Mather TA, Pyle DM, Lewi E, Yirgu G, Caliro S, Chiodini G, Clor LE, Fischer TP (2016) Causes of unrest at silicic calderas in the East African Rift: new constrains from InSAR and soil-gas chemistry at Aluto volcano, Ethiopia. Geochem Geophys Geosyst 17(8):3008–3030. https://doi.org/10.1002/2016GC006395.Received

Johnstrup JF (1877) Om de året 1875 forefaldne vulcanske Udbrud paa Island. Geogr Tidsskr 1:50–66

Lagabrielle Y, Garel E, Dauteuil O, Cormier M-H (2001) Extensional faulting and caldera collapse in the axial region of fast spreading ridges: analog modeling. J Geophys Res 106(B2):2005–2015. https://doi.org/10.1029/2000JB900266

Lupi M, Geiger S, Carey RJ, Thordarson T, Houghton BF (2011) A model for syn-eruptive groundwater flow during the phreatoplinian phase of the 28-29 March 1875 Askja volcano eruption, Iceland. J Volcanol Geotherm Res 203(3-4):146–157. https://doi.org/10.1016/j.jvolgeores.2011.04.009

Nobile A, Pagli C, Keir D, Wright TJ, Ayele A, Ruch J, Acocella V (2012) Dike-fault interaction during the 2004 Dallol intrusion at the northern edge of the Erta Ale Ridge (Afar, Ethiopia). Geophys Res Lett 39(19):2–7. https://doi.org/10.1029/2012GL053152

Pagli C, Sigmundsson F, Árnadóttir T, Einarsson P, Sturkell E (2006) Deflation of the Askja volcanic system: constraints on the deformation source from combined inversion of satellite radar interferograms and GPS measurements. J Volcanol Geotherm Res 152(1-2):97–108. https://doi.org/10.1016/j.jvolgeores.2005.09.014

Pagli C, Wright TJ, Ebinger CJ, Yun SH, Cann JR, Barnie T, Ayele A (2012) Shallow axial magma chamber at the slow-spreading Erta Ale Ridge. Nat Geosci 5(4):284–288. https://doi.org/10.1038/ngeo1414

Perlt J, Heinert M, Niemeier W (2008) The continental margin in Iceland—a snapshot derived from combined GPS networks. Tectonophysics 447(1-4):155–166. https://doi.org/10.1016/j.tecto.2006.09.020

Rubin AM (1992) Dike-induced faulting and graben subsidence in volcanic rift zones. J Geophys Res 97(B2):1839–1858. https://doi.org/10.1029/91JB02170

Ruch J, Walter TR (2010) Relationship between the InSAR-measured uplift, the structural framework, and the present-day stress field at Lazufre volcanic area, central Andes. Tectonophysics. https://doi.org/10.1016/j.tecto.2010.06.003

Ruch J, Wang T, Xu W, Hensch M, Jónsson S (2016) Oblique rift opening revealed by reoccurring magma injection in central Iceland. Nat Commun 7:1–7. https://doi.org/10.1038/ncomms12352

Rymer H, Locke C, Ófeigsson BG, Einarsson P, Sturkell E (2010) New mass increase beneath Askja volcano, Iceland—a precursor to renewed activity? Terra Nov 22:309–313. https://doi.org/10.1111/j.1365-3121.2010.00948.x

Saemundsson K (1991) The geology of the Krafla system. Garðarsson A, Einarsson A Náttúra My´ vatns Hið íslenska náttúrufraeðifélag, Reykjavík 25–95

Schöpa A, Burtin A, Hovius N, Green RG (2016) Dynamics of the Askja caldera landslide, July 2014, from seismic signal analysis

Sella GF, Dixon TH, Mao A (2002) REVEL: a model for recent plate velocities from space geodesy. J Geophys Res 107(B4):1–31. https://doi.org/10.1029/2000JB000033

Sigmundsson F (2006) Iceland geodynamics: crustal deformation and divergent plate tectonics. Reykjavik

Sigmundsson F, Hreinsdóttir S, Hooper A, Árnadóttir T, Pedersen R, Roberts MJ, Óskarsson N, Auriac A, Decriem J, Einarsson P, Geirsson H, Hensch M, Ófeigsson BG, Sturkell E, Sveinbjörnsson H, Feigl KL (2010) Intrusion triggering of the 2010 Eyjafjallajökull explosive eruption. Nature 468(7322):426–430. https://doi.org/10.1038/nature09558

Sigmundsson F, Hooper A, Hreinsdóttir S, Vogfjörd KS, Ófeigsson BG, Heimisson ER, Dumont S, Parks M, Spaans K, Gudmundsson GB, Drouin V, Árnadóttir T, Jónsdóttir K, Gudmundsson MT, Högnadóttir T, Fridriksdóttir HM, Hensch M, Einarsson P, Magnússon E, Samsonov S, Brandsdóttir B, White RS, Ágústsdóttir T, Greenfield T, Green RG, Hjartardóttir ÁR, Pedersen R, Bennett RA, Geirsson H, la Femina PC, Björnsson H, Pálsson F, Sturkell E, Bean CJ, Möllhoff M, Braiden AK, Eibl EPS (2014) Segmented lateral dyke growth in a rifting event at Bárðarbunga volcanic system, Iceland. Nature 517:15. https://doi.org/10.1038/nature14111

Sigvaldason GE (1979) Rifting, magmatic activity and interaction between acid and basic liquids: the 1875 Askja eruption in Iceland

Sigvaldason GE (2002) Volcanic and tectonic processes coinciding with glaciation and crustal rebound: an early Holocene rhyolitic eruption in the Dyngjufjoll volcanic centre and the formation of the Askja caldera, north Iceland. Bull Volcanol 64(3-4):192–205. https://doi.org/10.1007/s00445-002-0204-7

Sturkell E, Sigmundsson F (2000) Continuous deflation of the Askja caldera, Iceland, during the 1983–1998 noneruptive period. J Geophys Res 105(B11):25671–25684. https://doi.org/10.1029/2000JB900178

Sturkell E, Sigmundsson F, Slunga R (2006) 1983-2003 decaying rate of deflation at Askja caldera: pressure decrease in an extensive magma plumbing system at a spreading plate boundary. Bull Volcanol 68(7-8):727–735. https://doi.org/10.1007/s00445-005-0046-1

Thordarson T, Larsen G (2007) Volcanism in Iceland in historical time: volcano types, eruption styles and eruptive history. J Geodyn 43(1):118–152. https://doi.org/10.1016/j.jog.2006.09.005

Trippanera D, Acocella V, Ruch J, Abebe B (2015) Fault and graben growth along active magmatic divergent plate boundaries in Iceland and Ethiopia. Tectonics 34(11):2318–2348. https://doi.org/10.1002/2015TC003991

Tryggvason E (1984) Widening of the Krafla fissure swarm during the 1975-1981 volcano-tectonic episode. Bull Volcanol 47(1):47–69. https://doi.org/10.1007/BF01960540

Vogfjörd K, Helgason JK, Jonsdottir K, et al (2015) The Askja rockslide and the associated tsunami in the caldera lake

Wadge G, Burt L (2011) Stress field control of eruption dynamics at a rift volcano: Nyamuragira, D.R. Congo. J Volcanol Geotherm Res 207(1-2):1–15. https://doi.org/10.1016/j.jvolgeores.2011.06.012

Walker GPL (1958) Geology of the Reydarfjordur area, eastern Iceland. Q J Geol Soc 114(1-4):367–391. https://doi.org/10.1144/gsjgs.114.1.0367

Walker GPL (1963) The Breiddalur central volcano, eastern Iceland. Q J Geol Soc 119(1-4):29–63. https://doi.org/10.1144/gsjgs.119.1.0029

Walker GPL (1974) The structure of eastern Iceland. Geodyn Icel North Atl Area, Proc NATO Adv Study Inst Held Reykjavík, Iceland, 1–7 July 1974, Ed by L Kristjansson 177–188. https://doi.org/10.1007/978–94–010-2271-2_12

Wauthier C, Cayol V, Smets B, d'Oreye N, Kervyn F (2015) Magma pathways and their interactions inferred from InSAR and stress modeling at Nyamulagira volcano, D.R. Congo. Remote Sens 7(11):15179–15202. https://doi.org/10.3390/rs71115179

Wright TJ, Sigmundsson F, Pagli C, Belachew M, Hamling IJ, Brandsdóttir B, Keir D, Pedersen R, Ayele A, Ebinger C, Einarsson P, Lewi E, Calais E (2012) Geophysical constraints on the dynamics of spreading centres from rifting episodes on land. Nat Geosci 5(4):242–250. https://doi.org/10.1038/ngeo1428